Journal of Power Sources 261 (2014) 75–85

Contents lists available at ScienceDirect

Journal of Power Sources

journal homepage: www.elsevier.com/locate/jpowsour

# Semi-closed tubular light-trapping geometry dye sensitized solar cells with stable efficiency in wide light intensity range

Wei Zeng [a], Mingjun Wang [a], Yuan Li [b], Jiawei Wan [a], Huihui Huang [a], Hong Tao [a], David L. Carroll [b], Xingzhong Zhao [a], Dechun Zou [c], Guojia Fang [a,*]

[a] Key Laboratory of Artificial Micro- and Nano-structures of Ministry of Education of China, Department of Electronic Science and Technology, School of Physics and Technology, Wuhan University, Wuhan 430072, PR China
[b] Center for Nanotechnology and Molecular Materials, Department of Physics, Wake Forest University, Winston-Salem, NC 27109, USA
[c] Beijing National Laboratory for Molecular Sciences, Key Laboratory of Polymer Chemistry and Physics of the Ministry of Education, College of Chemistry and Molecular Engineering, Peking University, Beijing 100871, PR China

## HIGHLIGHTS

- A semi-closed tube dye sensitized solar cell serves as a light-trapping.
- The solar cell shows relatively stable efficiency in wide light intensity range.
- The light absorption is calculated with Fresnel equation and iterative approach.
- The optical paths in light-trapping are clearly presented.
- The solar cell has potential as effective collector in converged light system.

## GRAPHICAL ABSTRACT

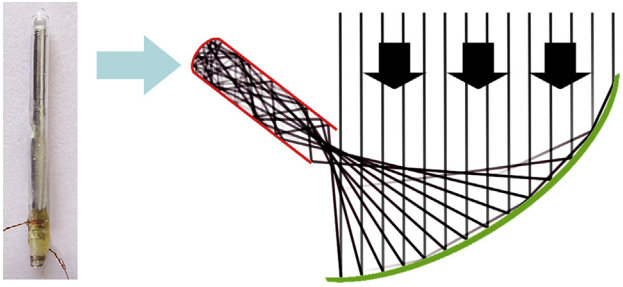

## ARTICLE INFO

*Article history:*
Received 1 February 2014
Accepted 14 March 2014
Available online 25 March 2014

*Keywords:*
Dye sensitized solar cell
Tube structure
Light-trapping
Light intensity
Charge transport
Heat dissipation

## ABSTRACT

A semi-closed tubular light-trapping geometry is developed for dye sensitized solar cell to stabilize its power conversion efficiency (PCE) in wide light intensity range. The tubular cell consists of a dye-sensitized porous $TiO_2$ coated and semi-closed glass tube as photoanode, an opaque platinum metal foil wrapped on the outside of photoanode as counter electrode, and electrolyte filling in their interlayer. The open end of photoanode serves as the only light entrance. The experiment, calculation and optical studies demonstrated that the tubular geometry is beneficial to light trapping and absorption, charge transport and heat dissipation, in comparison to a planar counterpart. The PCE of tubular cell can remain about 85% of its original value even if the irradiated light intensity increases from 1 to 5 Sun, in contrast, that of planar counterpart decreases to about 60% of its original value. This feature makes the tubular cell has potential as an effective light collector in low-cost condenser solar cell system.



## 1. Introduction

Nowadays, photoelectric conversion has been one of attractive methods to generate clean energy instead of the conventional fossil energy. The silicon solar cells have been widely applied in daily life. For lower cost and environmental protection, other types

* Corresponding author.
*E-mail address:* gjfang@whu.edu.cn (G. Fang).

http://dx.doi.org/10.1016/j.jpowsour.2014.03.050
0378-7753/

of solar cells, such as dye sensitized solar cells (DSSCs) [1,2], organic solar cells [3,4] and perovskite solar cells [5], have been explored. Improvement of their power conversion efficiency (PCE) is one of persistent research interests. In practical applications, more output electric power generally needs expensive large–scale solar cells to harvest more light. In contrast, converging large–scale lights on a small–scale solar cell is one of low–cost methods [6]. It can be carried out by bifacial irradiation, diffuse reflection technologies [7,8] or a condenser solar cell system [9,10]. A typical condenser solar cell system consists of several elements, essentially including an optical condenser, collector, thermal dissipation equipment, support equipment and tracking equipment. The condenser could be either reflective or refractive with large irradiated area for converging sunlight, and the collector is a solar cell for conversion of light energy into electric energy [11]. Many types of solar cells are appropriate as collector in this system [11,12]. However, in the case of intense illumination, the solar cell collector suffers several problems. Many irradiated light will be lost by light reflection or penetration [13]. The charge diffusion in electrochemical solar cell will be limited [14]. In addition, large amount of heat will be generated [12,15]. These problems will low down the PCE of solar cell, and then reduce the total energy harvest of system.

In the study of DSSC, a series of works are reported to stabilize the PCE of cell in intense illumination. Many works are carried out for common cells in planar geometry. The avoiding irradiated light loss is one of the main methods. Two planar DSSCs are proposed to form a laminated structure for reusing the light penetrating through cell [16], and a extra light scattering layer is introduced on photoanode for reflecting light back [9]. In addition, charge recombination is proposed an important affecting factor on cell performance in intense light intensity [17–19]. On the other hand, some related works have been reported for avoiding light loss in the case of 1 Sun illumination (100 mW $cm^{-2}$). They are available references for the study in intense illumination. An antireflection layer is proposed to be coated on the irradiated side of cell [20–22]. A reflector layer is proposed to be coated below the cell [23]. The light absorption layer in photoanode is proposed to form a three–dimensional light-trapping nanostructure, such as microcavity–embedded structure [13], photonic crystal structure [24] and plasmon resonance structures [25]. The light-trapping nanostructure reveals promising prospect. The calculated result reveals that the light-trapping of photonic crystal can even provide at least a factor of one–third enhancement in solar light absorption and PCE relative to the conventional counterparts [26]. However, the preparation processes of these light-trapping nanostructures are relatively complex. A simpler method to form light-trapping is reported. It is carried out by directly changing cell geometry from planar to curve. The reported main curve geometry for DSSC is fiber and tube to our knowledge [27,28]. In 1 Sun illumination, the fiber light-trapping geometry is demonstrated beneficial to light absorption when one of its ends is irradiated [29,30]. Tubular DSSCs with side irradiations were reported in literature [31,32]. However, light-trapping effect is not fully demonstrated in those tubular DSSCs. For lower cost and higher energy harvest in condenser solar cell system, this type of simple light-trapping geometry solar cell is required, and investigation on its light-trapping and photocurrent density–voltage ($J$–$V$) characteristics at intense light intensity condition is necessary.

In this paper, a semi-closed tubular geometry is developed for DSSC device. The tubular cell (TCell) consists of a dye–sensitized porous $TiO_2$ coated and semi-closed glass tube as photoanode, an opaque platinum (Pt) metal foil wrapped on the outside of photoanode as counter electrode (CE), and electrolyte filling in their interlayer. The open end of photoanode serves as the only light entrance. The effects of tubular feature such as the thickness and length of porous $TiO_2$ layer (PTL), as well as light incidence angle on cell PCE are discussed based on experiment, calculation and optical path studies. The semi-closed tubular light-trapping geometry is demonstrated beneficial to light absorption, charge transport and heat dissipation, in comparison to a planar counterpart. Even if the light intensity increases from 1 to 5 Sun, the PCE of TCell can remain about 85% of its original value, in contrast, that of planar counterpart decreases to about 60% of its original value. Such feature makes the TCell has potential as an effective collector in economical condenser solar cell system.

## 2. Materials and methods

### 2.1. Materials

Tetrabutyl titanate, diethanol amine, ethanol, hydrochloric acid, nitric acid, glacial acetic acid, polyethylene glycol, acetonitrile and valeronitrile were obtained from Sinopharm Chemical Reagent Corporation (China). 1-methyl-3-propyl imidazolium iodide (PMII), Iodine ($I_2$), 4-tert-butylpyridine (TBP) and guanidine thiocyanate (GuSCN) were purchased from Aladdin-reagent. The Ru dye of (cis-di(thiocyanato)- N–N′-bis(2,2′-bipyridyl -4-carboxylic acid-4 -tetrabutylammonium carboxylate) ruthenium (II) (N719) was purchased from Solaronix (Switzerland). Lithium iodide (LiI, 99.99%) and titanium isopropoxide were obtained from Acros. All the reagents not indicated were of analytical purity. Glass tubes with a closed hemispherical end were obtained from Chemglass. The inner diameter, wall and outer diameter of the tube are 0.8, 0.25 and 1.3 mm, respectively.

### 2.2. Preparation of DSSC

#### 2.2.1. Preparation of tubular DSSCs

A tubular photoanode is fabricated as follow. In advance, a dense $TiO_2$ sol and a porous sol were prepared with a method referring to literature [33,34], and glass tubes were cleaned in ultrasonic bath with ethanol, acetone and deionized water in sequence. Then, an indium tin oxide (ITO) film was deposited on the entire outer surface of tube by a magnetron sputtering system. After a layer of dense $TiO_2$ sol was coated on the tube with dip–coating method, the sample was sintered at 500 °C for 15 min, and then a dense $TiO_2$ layer (DTL) is obtained. When the sample was cooled down to room temperature, a layer of porous $TiO_2$ sol was coated on the tube with dip–coating method. After the sample was sintered at 500 °C for 15 min, a PTL was obtained. The PTL thickness can be controlled by the concentration of porous $TiO_2$ sol and repetitive times of the coating and sintering procedures. Finally, the electrodes were rinsed with ethanol and then dipped into 0.3 mM N719 ethanol solution at 60 °C for 12 h.

A TCell is assembled as follow. Firstly, a thin copper wire was twined on the ITO layer on photoanode, and then wrapped by a Teflon tape. This copper wire serves as a test connector for photoanode. Then, a Pt foil of 0.05 mm thickness, served as CE, was rolled on the entire photoanode including its closed end. Another thin copper wire was twined on the Pt foil, and then wrapped by a Teflon tape. It acts as a test connector for CE. When the electrolyte was dropped into the interface of photoanode and CE, these wrapped components were inserted into another semi-closed glass tube with relatively larger inner diameter, which was just used as an outer seal container. Finally, the joint between the two tubes at the opening end part was sealed with ethoxyline resin.

*2.2.2. Preparation of planar DSSCs*

A planar photoanode is fabricated with the same working procedures as those described for TCells. The only difference is that the planar photoanode employs planar substrate, which is planar glass coated by transparent conducting oxide (TCO) layer, such as ITO or fluorine doped tin oxide (FTO) layer. A PCell is assembled as follow. Firstly, its photoanode and CE are tightly put together. Then, the electrolyte was dropped into their interface. Lastly, the edge between photoanode and CE is sealed with ethoxyline resin.

*2.3. Characteristics*

The morphology and structure were investigated by using a scanning electron microscopy (Sirion SEM, FEI, Netherlands). The transmission spectrum of film was measured by an ultraviolet–visible–near infrared radiation spectro–photometer (CARY 5000, Varian, Australia) in the 300–900 nm wavelength range at room temperature. The sheet resistance of ITO was measured by a four point probe method. The *J–V* characteristics of DSSC devices were measured using an AM1.5G standard Newport No. 96000 Solar Simulator. The illumination intensity can be tuned by adjusting the input current of solar simulator. Current voltage characteristics were collected using a Keithley 2400 source measurement unit.

In *J–V* test, the location of light source is invariable, and the different light incidence angle ($\theta$) is formed by different gradient of tested device. For clear presentation, the test posture for TCells is drawn in Fig. 1(a). With this irradiation method, the opening end of TCell serves as the only light entrance, because the entire tube wall is shielded by opaque Pt CE. At different $\theta$ values, the irradiated area for calculation of photocurrent density is defined as a constant. The value is the cross section area of the photoanode hole at the opening part, and it is $5.0 \times 10^{-3}$ cm$^2$. This irradiated area is signed in shaded in Fig. 1(b) for clear exhibition. The test posture for PCells is shown in Fig. 1(c), where the $\theta$ is formed with the same method as that discribed for TCells. A PCell is covered by a metal mask with a round light hole. The irradiated area for PCell depends on the area of hole. Here, the irradiated area for PCell is also $5.0 \times 10^{-3}$ cm$^2$, which is the same as that of TCell.

Electrochemical impedance spectroscopy (EIS) was performed with a frequency ranging from 100 kHz to 0.1 Hz at open–circuit potential by using a CHI 660D electrochemical workstation (Shanghai, China). The cell position in the EIS measurement is the same as that of *J–V* measurement. The electrolyte is the same for both *J–V* and EIS measurements. It is a solution of 1 M PMII, 0.04 M LiI, 0.03 M $I_2$, 0.1 M GuSCN and 0.5 M TBP in a mixture of acetonitrile and valeronitrile (volume ratio, 85:15).

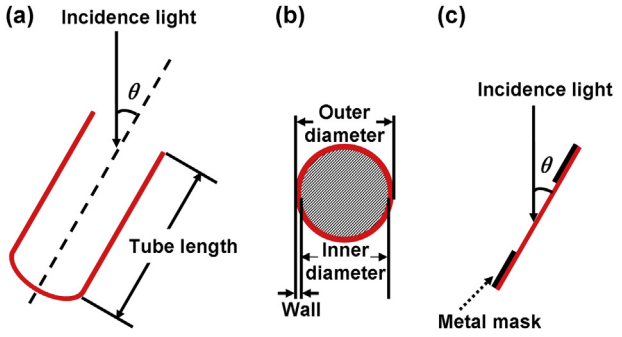


**Fig. 1.** (a) The posture for TCells under *J–V* test with light incidence angle of $\theta$. (b) The cross–section diagram of a glass tube. The shaded region indicates the irradiated area. (c) The posture for PCells under *J–V* test with light incidence angle of $\theta$.

## 3. Calculation

The light absorption power of tube wall is calculated with a method described as follows. The effects from two optical interfaces are studied. One interface is between air and glass layer, and another is between glass and ITO layers. At each interface, light reflection and refraction both occur, and the reflection and refraction light share the total power of incidence light. The light power segmentation is calculated based on Fresnel equation and iterative approach. The different $\theta$ value signifies different share ratios. The detailed calculation process has been presented in our previous reported work [35–37]. The light power absorbed by PTL indicates the effective light absorption power of device ($P_A$). It is given by $P_A = P_{IN} - P_{OUT} - P_{LOSS}$. The $P_{IN}$ and $P_{OUT}$ indicate the light powers which enter tube cavity from the irradiated end and that exits from the rear opening end, respectively. The $P_{LOSS}$ indicates the losing light power, which is the light power absorbed by glass or ITO layers [36]. The $P_{IN}$ is given by $P_{IN} = P_{IRRA}\cos\theta$, where the $P_{IRRA}$ is the irradiated light intensity generated by the Solar Simulator. Compared to $P_{IN}$ or $P_{OUT}$ value, the $P_{LOSS}$ value is much smaller [36], so the $P_{LOSS}$ value is ignored in the $P_A$ calculation and the $P_A$ value is just expressed as $P_A = P_{IN} - P_{OUT}$.

## 4. Results and discussion

*4.1. The description of TCell*

An as–fabricated TCell device consists of two nested semi-closed glass tubes. The inner tube serves as photoanode substrate and outer tube is just for encapsulation. As shown in Fig. 2(a), the photoanode including its closed end are entirely wrapped by Pt CE. The functional layers from the inner to outer in the device are ITO, DTL, dye/PTL, electrolyte and Pt in sequence, as shown in Fig. 2(b). A series of dyed–sensitized photoanodes with different tube lengths are photographed and shown in Fig. 2(c). It is clear that both tube wall and closed end part are entirely dyed, indicating they are both effective working regions of cell. A real sealed device is shown in Fig. 2(d).

The cross section of a tubular photoanode is observed by a SEM system as shown in Fig. 3(a). The functional layers can be distinguished. The thicknesses of ITO layer, DTL and PTL are measured to be about 189.4 nm, 94.7 nm and 3.3 μm, respectively. The ITO film with the same thickness is deposited on a glass slide for verification of its optical and electrical properties. Fig. 3(b) shows the transmission spectrum of this ITO film on glass slide. This spectrum

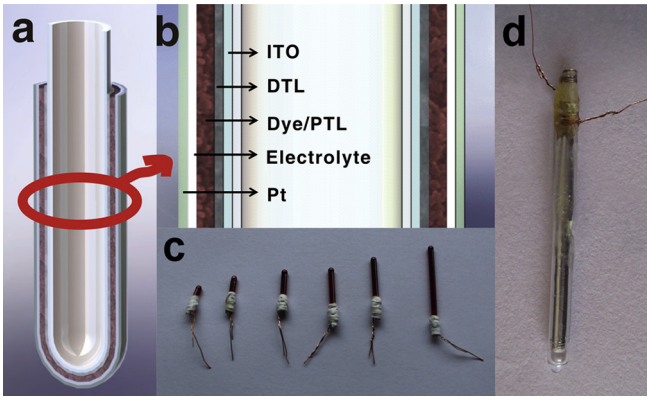


**Fig. 2.** (a) Configuration diagram for a TCell. (b) The detailed formation diagram for a TCell. (c) A photograph of dye sensitized tubular photoanodes with different tube lengths. (d) A photograph of a sealed TCell.

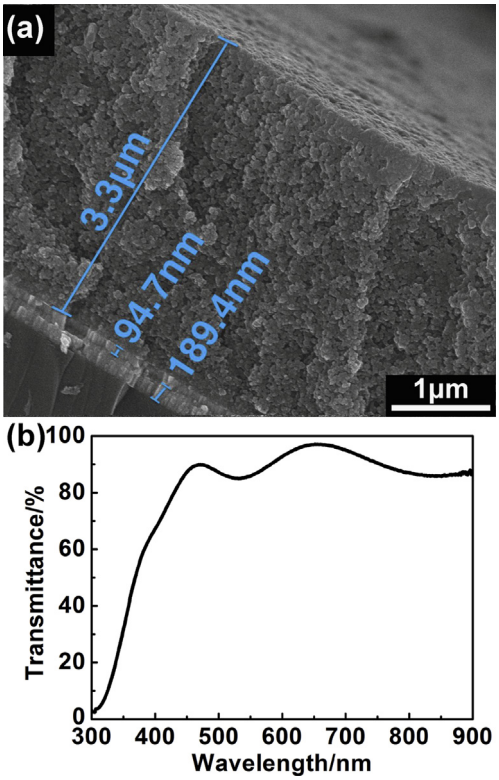


**Fig. 3.** (a) The SEM image for a tubular photoanode in cross–section view. (b) The transmission spectrum of ITO film on glass slide.

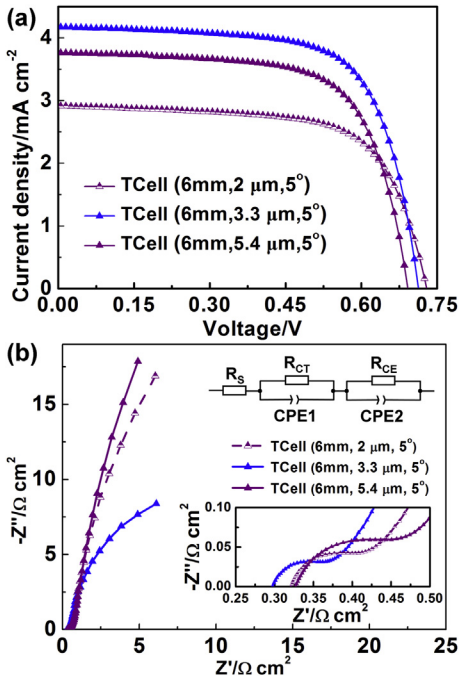


**Fig. 4.** (a) The *J–V* curves and (b) Nyquist plots of TCells with different PTL thickness. The insets of (b) are the equivalent circuit and enlarged plot in high frequency region.

reveals that this ITO film has an appreciable transmittance. When the ITO film is just sputtered, its sheet resistance is measured and it is about 60 Ω square$^{-1}$.

### 4.2. The feature of TCell

#### 4.2.1. The opening end

In literature report, a fiber cell has a solid structure with two opening ends [29,30]. In contrast, a semi-closed TCell fabricated here has a hollow structure with only one opening end. When one of opening ends in fiber cell is irradiated, part lights will be reflected away on this solid end. However, when the opening end of TCell is irradiated, the whole irradiated lights can enter the tube cavity without light reflection loss. Therefore, this type of tubular geometry is more beneficial for light incidence compared to fiber geometry.

#### 4.2.2. The PTL thickness of TCell

For planar or fiber DSSC device, PTL thickness is demonstrated a significant parameter on cell performance [38,39]. In order to obtain the optimized PTL thickness for TCells, we fabricate a series of TCells with the same tube length of 6 mm but different PTL thicknesses of 2, 3.3 and 5.4 μm. Their *J–V* and EIS are measured at the same $\theta = 5°$ for effective comparison. The effects from tube length and $\theta$ on cell performance will be discussed in the following sections. Their *J–V* curves are shown in Fig. 4(a) and detailed results are listed in Table 1. When the PTL thickness is 3.3 μm, the biggest PCE of 2.04% is achieved. Comparisons of $J_{SC}$, $V_{OC}$ and FF variation for these cells are made. It is observed that the $J_{SC}$ variation is the most remarkable, and the cell which gains the biggest PCE mainly depends on its biggest $J_{SC}$ value.

The Nyquist plots of these TCells are shown in Fig. 4(b). The equivalent circuit and enlarged curves in high frequency are shown in the top and bottom insets of Fig. 4(b), respectively. The $R_S$, $R_{CT}$, *CPE1* (or *CPE2*) and $R_{CE}$ mean the Ohm series resistance, charge–transfer resistance at CE/electrolyte interface, constant phase element and charge–transfer resistance at $TiO_2$/dye/electrolyte interface, respectively [40,41]. These parameters are fitted by Zview software and the fitted results are listed in Table 1. Comparisons of $R_S$, $R_{CT}$ and $R_{CE}$ variation are made. It is observed that the $R_{CE}$ variation is the most remarkable, and the cell which gains the biggest PCE has the smallest $R_{CE}$. A thinner PTL signifies less light–generated electrons [42], and a thicker PTL signifies longer diffusion distance for the light–generated electrons [43], *i.e.* the bigger charge recombination rate. It is reported that the $R_{CE}$ can increase in these two cases [43]. In other words, the $R_{CE}$ has a negative relationship with the amount of light–generated electron, and has a positive relationship with the charge recombination rate. Therefore, here the smallest $R_{CE}$ value can be attributed to its appropriate PTL thickness. In general, it is demonstrated that a smaller internal resistance ($R_S$, $R_{CT}$ or $R_{CE}$) of DSSCs is corresponding to higher cell performance [44]. For example, it is reported that a smaller $R_{CE}$ value is beneficial to the $J_{SC}$ or FF values for DSSCs [39,45], and the $R_S$, $R_{CT}$ or $R_{CE}$ value has a negative relationship with the PCE value [46]. Here, for these TCells, the $R_{CE}$ shows a negative relationship with the $J_{SC}$ or PCE value, which is in accordance with the literate report.

**Table 1**
The *J–V* characteristics and fitted equivalent resistances for TCells with different PTL thickness.

| PTL thickness (μm) | $V_{OC}$ (V) | $J_{SC}$ (mA cm$^{-2}$) | FF | PCE (%) | $R_S$ (Ω cm$^2$) | $R_{CT}$ (Ω cm$^2$) | $R_{CE}$ (Ω cm$^2$) |
|---|---|---|---|---|---|---|---|
| 2 | 0.74 | 2.91 | 0.66 | 1.42 | 0.32 | 0.10 | 43.3 |
| 3.3 | 0.72 | 4.17 | 0.68 | 2.04 | 0.30 | 0.10 | 21.5 |
| 5.4 | 0.70 | 3.76 | 0.67 | 1.76 | 0.33 | 0.12 | 41.5 |

*4.2.3. The light incidence angle*

To study the influence of tube length and $\theta$ on TCell performance, we fabricate a series of TCells. They have the same PTL thicknesses of 3.3 μm (as optimized above), but different tube lengths, and they are tested with different $\theta$ values in $J$–$V$ and EIS measurements. The relationship between PCE and $\theta$ by different tube lengths is summarized and shown in Fig. 5(a). The highest PCE of 2.54% is achieved by TCell with 3 mm tube length at $\theta = 5°$. The corresponding $V_{OC}$, $J_{SC}$ and FF values are 0.71 V, 5.77 mA cm$^{-2}$ and 0.62, respectively. This TCell is denoted as TCell-m in the following study for simplification. The tube wall is a necessary part of tube. The light power absorbed by tube wall is calculated. The relationship between $P_A$ and $\theta$ values by increasing tube length is shown in Fig. 5(b), where the $P_A$ values are normalized by their maximum value. For clear exhibition, the optical paths for tube walls and complete tubes at typical $\theta$ values are drawn in Fig. 6 according to their real sizes. The Nyquist plots of cells are shown in Fig. 7 and the corresponding equivalent resistances are listed in Table 2. The equivalent circuit of TCells with 1.7 mm tube length is shown in the inset of Fig. 7(a), and that of TCells with 3 and 6 mm tube length is shown in the inset of Fig. 4(b).

As shown in Fig. 5(b), with the same tube length, it is observed that the $P_A$ firstly increases from zero to the maximum value when the $\theta$ increases from 0° to about 5°, and then it decreases to zero when the $\theta$ increases to 90°. The results can be illustrated with optical path analysis as follows. With the same tube length of 3 mm, the optical paths of tube walls at typical $\theta$ values of 0, 5 and 45° are shown in Fig. 6(a), (b) and (c), respectively. It is observed that incidence light ($P_{IN}$) decreases with increasing $\theta$ value. In Fig. 6(a), all entered rays exhaustively exit, indicating $P_{IN} = P_{OUT}$. This explains the $P_A = 0$ at $\theta = 0°$ in Fig. 5(b). In addition, no rays can enter the cell at $\theta = 90°$, indicating $P_{IN} = 0$. This explains the $P_A = 0$ at $\theta = 90°$ in Fig. 5(b). In Fig. 5(b), the maximum $P_A$ is achieved at $\theta \approx 5°$, which can be attributed to the compromise of $P_{IN}$ and $P_{OUT}$ variations.

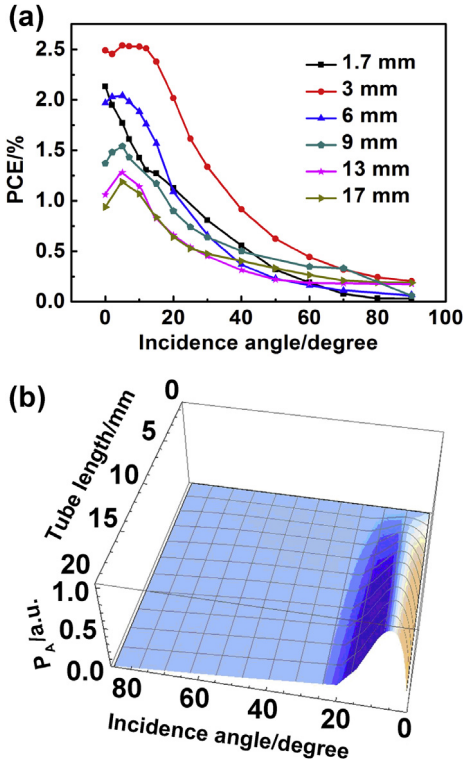


**Fig. 5.** (a) The experimental results of the PCE *vs* light incident angle for TCells, by different tube length, with 3.3 μm PTL thickness. (b) The calculation results of the light absorption power *vs* light incident angle for tube walls, by different tube length.

With the same tube length of 3 mm, the optical paths of complete tube geometry at different $\theta$ values of 0, 5 and 45° are shown in Fig. 6(d), (e) and (f), respectively. The optical path comparisons between the tube wall and corresponding complete tube at the same $\theta$ are made. At the same $\theta$ value, it is clear that the closed end effectively prevents lights from leaking out. Therefore, the $P_A$ value of complete tube is bigger than that of tube wall at the same $\theta$ value. This role of closed end is especially obvious at a smaller $\theta$ value, such as 0 or 5°, as shown in Fig. 6(d) and (e). At a relatively bigger $\theta$ value, the role of closed end is weak, because most light power can be absorbed by tube wall during multiple light reflections, as shown in Fig. 6(f). In addition, as shown in Fig. 5(a) and (b), it is at the same $\theta = 5°$ that the PCE of complete TCell and the $P_A$ of tube wall both achieve their maximum values. This reveals that the light absorption of tube wall plays important role on cell PCE.

In the case of the same tube length, comparisons of the equivalent resistances for these TCells are made. As shown in Table 2 and Fig. 5(a), with the same tube length, it is observed that the $R_{CE}$ variation is the most remarkable, and the $R_{CE}$ shows a negative relationship with the PCE. This relationship between $R_{CE}$ and PCE further confirms the result deduced in Section 4.2.2. When the tube length is 3 or 6 mm, the minimum $R_{CE}$ is achieved at $\theta = 5°$. As mentioned above of this section, it is just $\theta = 5°$ where the $P_A$ of tube wall get the maximum value. A bigger $P_A$ reveals more light–generated electrons. Therefore, it can be deduced that here the smaller $R_{CE}$ can be mainly attributed to the bigger $P_A$ (or more light–generated electrons). When the tube length is only 1.7 mm, the minimum $R_{CE}$ is achieved at $\theta = 0°$ but not $\theta = 5°$, which does not meet the regularity deduced above. When the complete tube is 1.7 mm length, the lights can be reflected out of the tube cavity from the irradiated opening end, as shown in Fig. 6(i). Therefore, this irregularity can be attributed to its too short tube length, which makes the TCell unable be regarded as an effective light-trapping.

*4.2.4. The tube length*

The effect of tube length on $P_A$ value for tube wall is described in Fig. 5(b). It is observed that the $P_A$ value increases with increasing tube length at a fixed $\theta$ value. This can be illustrated with optical path analysis as follows. At the same $\theta = 5°$, the optical paths of tube walls with 1.7, 3.3 and 6 mm tube lengths are shown in Fig. 6(g), (b) and (h), respectively. It is illustrated that more incidence lights are received on longer tube wall. Therefore, a bigger $P_A$ value (or more photo–generated electrons) can be obtained with longer tube wall. At the same $\theta = 5°$, the optical paths of complete tube geometries with 1.7, 3 and 6 mm tube lengths are shown in Fig. 6(i), (e) and (j), respectively. It is illustrated that the lights can be reflected more times in longer complete tube until they are entirely absorbed, indicating the light absorption opportunity increases with increasing tube length. This reveals that the $P_A$ can increase with increasing tube length for complete tubes, until the $P_A$ reaches its maximum. With the same tube length, the optical path comparisons between tube wall and complete tube are made. It is clear that the lights can not be leaked out from the rear closed end, but they have opportunity to escape from the irradiated opening end by light reflection. This escape has been discussed in Section 4.2.3. In general, with the same tube length, the complete tube is more beneficial to light absorption compared to tube wall because of its semi-closed geometry.

As shown in Fig. 5(a), at a fixed $\theta$ value, the experiment result shows that the PCE of TCell generally firstly increases and then decreases with increasing tube length, and the maximum PCE is achieved by the TCell with 3 mm tube length. Comparisons of the equivalent resistances for these TCells at the same $\theta$ value are made.

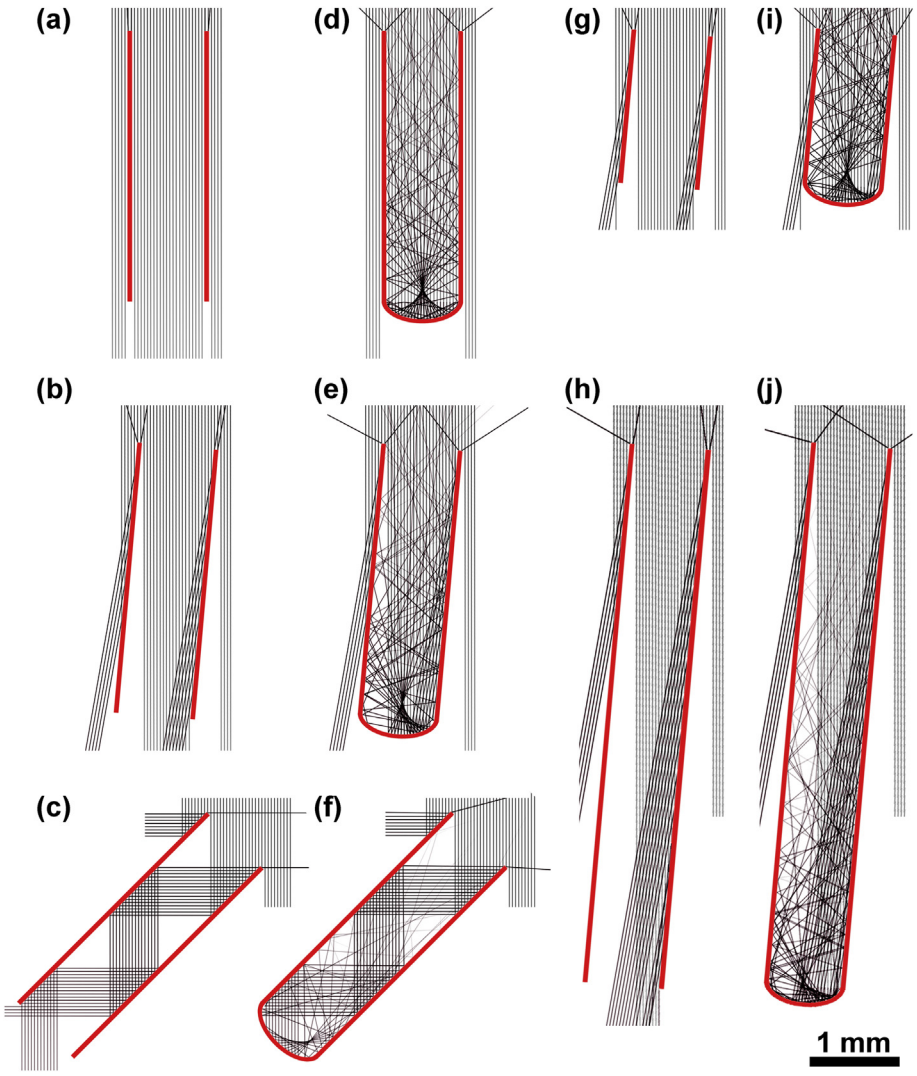


**Fig. 6.** The optical paths for tube walls and complete tube geometries. (a) tube wall, $\theta = 0°$, $L = 3$ mm. (b) tube wall, $\theta = 5°$, $L = 3$ mm. (c) tube wall, $\theta = 45°$, $L = 3$ mm. (d) tube, $\theta = 0°$, $L = 3$ mm. (e) tube, $\theta = 5°$, $L = 3$ mm. (f) tube, $\theta = 45°$, $L = 3$ mm. (g) tube wall, $\theta = 5°$, $L = 1.7$ mm (h) tube wall, $\theta = 5°$, $L = 6$ mm. (i) tube, $\theta = 5°$, $L = 1.7$ mm (j) tube, $\theta = 5°$, $L = 6$ mm. The $L$ signs tube length. The bar in bottom right corner is for real size.

At a fixed $\theta$ value, the $R_S$ or $R_{CT}$ values increases with increasing tube length. The increase of $R_S$ can be attributed to the increase of tube length, because the electrons need pass longer distance in longer tube to arrive outer circuit. The increase of $R_{CT}$ can also be attributed to the increase of tube length, because the $R_{CT}$ can be positively affected by $R_S$ [44]. At a fixed $\theta$ value, the $R_{CE}$ decreases with increasing tube length. As discussed above of this section, bigger $P_A$ can be obtained in longer complete tube until the $P_A$ reaches its maximum. In addition, bigger charge recombination rate can be obtained in longer complete tube because of bigger cell area. As discussed in Section 4.2.2 and 4.2.3, the $R_{CE}$ has a negative relationship with the $P_A$, and has a positive relationship with the charge recombination rate. Therefore, here the decreasing $R_{CE}$ can be attributed to the dominant effect of increasing $P_A$. According to the relationship between internal resistance and cell performance as discussed in Section 4.2.2, the resulting PCE variation here can be attributed to the two competitive affecting factors, *i.e.* $R_S$ (or $R_{CT}$) and $R_{CE}$ values. When the tube is too short such as 1.7 mm, the smaller PCE can be attributed to the dominant negative effect of bigger $R_{CE}$, which is caused by smaller $P_A$. When the tube is too long such as 6 mm, the smaller PCE can be attributed to the dominant negative effect of bigger $R_S$ (or $R_{CT}$), which is caused by bigger cell area. Therefore, when the tube is 3 mm length, the biggest PCE is due to the compromise of the two affecting factors.

### 4.3. Performance comparison of TCell and PCell under 1 Sun light intensity

#### 4.3.1. The effects of photoanode structure

In our previous reported works, the optimized PCE of a planar DSSC with Pt CE is about 6% under 1 Sun illumination [44,47]. However, in this work the PCE values of TCells are much smaller. The possible reason is analyzed as follow.

In our previous reported works, the PTL thickness is about 14 μm. However, the PTL thickness of optimized TCell, *i.e.* TCell-m, is only 3.3 μm, which is smaller than that of PCell. On the basis of discuss in Section 4.2.2, the thinner PTL maybe a reason for the much lower PCE of TCell-m.

In our previous reported works, the photoanode substrate is a commercial FTO glass. Its sheet resistance is about 14 Ω square$^{-1}$. This FTO substrate can undergo annealing in high temperature. In this work, the TCO layer of TCell-m is ITO fabricated by magnetron

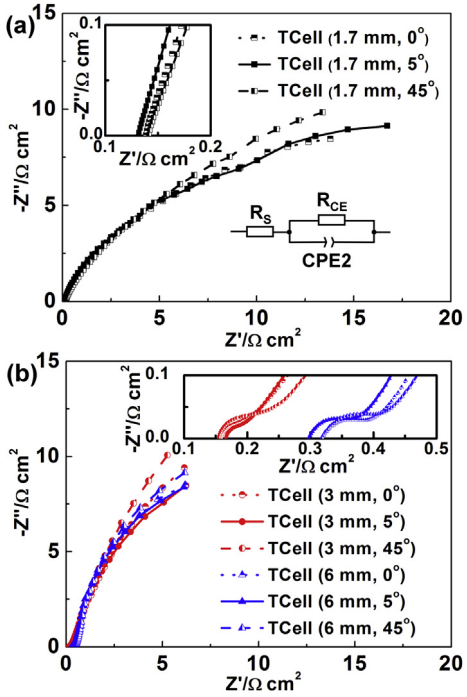


**Fig. 7.** (a) The Nyquist plots of TCells with 1.7 mm tube length and different test $\theta$ values. The insets are the equivalent circuit and enlarged plots in high frequency region. (b) The Nyquist plots of TCells with 3 and 6 mm tube lengths at different test $\theta$ values. The inset is enlarged plots in high frequency region.

sputtering. The PTL of TCell-m is fabricated by two times of porous $TiO_2$ coating and annealing processes. Therefore, the ITO layer on TCell-m undergoes three times of annealing, one of which is for DTL fabrication and other two are for PTL fabrication. Before the ITO–sputtered glass is annealed, its sheet resistance is about 60 Ω square$^{-1}$, as mentioned in Section 4.1. After this glass is annealed at 500 °C for 15 min with three times, it is observed that the ITO sheet resistance increases to about 200 Ω square$^{-1}$, indicating the high temperature anneal increases the ITO sheet resistance. The 200 Ω square$^{-1}$ may be the real sheet resistance of ITO layer for tested TCells. The sheet resistance of this ITO film is much bigger than that of the FTO, which maybe a reason for the much lower PCE of TCell-m.

In addition, in our previous reported works, the photoanode and CE for PCell are tightly put together, as mentioned in Section 2.2.2. In this work, the diameter of tubular photoanode is very small but the wrapped Pt metal foil CE is stiff. Therefore, an inevitable gap exists between the photoanode and CE in TCell, which maybe also a reason for the much lower PCE of TCell-m.

**Table 2**
The fitted equivalent resistances for TCells with the same PTL thickness of 3.3 μm but different tube length and different test $\theta$ value.

| Tube length (mm) | Test $\theta$ value (°) | $R_S$ (Ω cm$^2$) | $R_{CT}$ (Ω cm$^2$) | $R_{CE}$ (Ω cm$^2$) |
|---|---|---|---|---|
| 1.7 | 0 | 0.13 | – | 29.0 |
| 1.7 | 5 | 0.12 | – | 30.0 |
| 1.7 | 45 | 0.13 | – | 31.5 |
| 3 | 0 | 0.16 | 0.05 | 28.6 |
| 3 | 5 | 0.17 | 0.04 | 27.5 |
| 3 | 45 | 0.15 | 0.10 | 29.8 |
| 6 | 0 | 0.32 | 0.08 | 22.5 |
| 6 | 5 | 0.30 | 0.10 | 21.5 |
| 6 | 45 | 0.32 | 0.11 | 28.8 |

For exploring the influences of PTL thickness, TCO sheet resistance and gap width on cell performance, a series of contrast experiments are carried out. The experiments are carried out on PCells for simplification. Three different kinds of planar photoanodes are fabricated, and relevant PCells are assembled. A PCell is fabricated and denoted as PCell-F-t. Its photoanode is fabricated with the parameters described in our previous reported works [44,47]. Its CE is the flat Pt foil which is the same as that used in TCell-m. The second PCell is denoted as PCell-F. The only difference between PCell-F and PCell-F-t is PTL thickness. The PTL thickness of PCell-F is only 3.3 μm, which is the same as that of TCell-m for comparison. The third PCell is denoted as PCell-I. The only difference between the PCell-I and PCell-F is photoanode substrate. The photoanode substrate of PCell-I is the as–annealed ITO–sputtered glass fabricated by magnetron sputtering. The photoanode of PCell-I can be regarded as a flatted photoanode of TCell-m. The detailed geometry parameters of these PCells are listed in Table 3.

The $J$–$V$ characteristics of these PCells are measured and listed in Table 3. The tested $\theta$ and irradiated area of these PCells are both the same as those of TCell-m for comparison. It is observed that the PCE values of PCell-F-t, PCell-F and PCell-I are 6.18%, 5.71% and 2.67%, respectively. The PCE of PCell-F-t is close to that reported in our previous work [44]. Compared to PCell-F-t, the PCell-F shows smaller PCE mainly because of its smaller $J_{SC}$. The structure difference of PCell-F and PCell-F-t indicates that the smaller PCE (or smaller $J_{SC}$ value) of PCell-F is because the thinner PTL of PCell-F generates less photo–generated electrons [43]. Compared to PCell-F, the PCell-I shows smaller PCE. Comparisons of $V_{OC}$, $J_{SC}$ and FF variations for the two cells are made. It is observed that the FF variation is the most remarkable. The structure difference of PCell-I and PCell-F indicates that the much smaller PCE (or much smaller FF value) of PCell-I is because of its much bigger sheet resistance of TCO layer. Similar results were reported in literature [48–50].

### 4.3.2. The effects of gap width between photoanode and CE

The influence of gap width on cell performance is discussed as follows. The gap is deliberately generated by inserting a Teflon film between the photoanode and CE in original PCell-F. The gap width can be adjusted by changing the thickness of Teflon film. The gap–inserted cells are denoted as PCell-F-g1 and PCell-F-g2 when the thicknesses of Teflon film are 100 and 200 μm, respectively. Their $J$–$V$ characteristics are listed in Table 3. The PCE values of PCell-F, PCell-F-g1 and PCell-F-g2 are 5.71%, 4.91% and 4.38%, respectively. It is observed that the PCE decreases with increasing gap width. Comparisons of $J_{SC}$, $V_{OC}$ and FF variation for the three cells are made. The $V_{OC}$ and $J_{SC}$ variation are more remarkable, which may be attributed to the bigger resistance of electrolyte in wider gap [46]. A similar result has been reported in literature [51]. On the basis of discussions in Section 4.3.1 and 4.3.2, it can be summarized that the PCE varies positively to the PTL thickness, but inversely to TCO sheet resistance and gap width for PCells.

**Table 3**
The geometry parameters and $J$–$V$ characteristics of PCells with different photoanode structure and different gap width.

| Cell | TCO | Sheet resistance of TCO (Ω square$^{-1}$) | PTL thickness (μm) | Gap width (μm) | $V_{OC}$ (V) | $J_{SC}$ (mA cm$^{-2}$) | FF | PCE (%) |
|---|---|---|---|---|---|---|---|---|
| PCell-F-t | FTO | 14 | 14 | – | 0.68 | 14.65 | 0.62 | 6.18 |
| PCell-F | FTO | 14 | 3.3 | – | 0.67 | 13.97 | 0.61 | 5.71 |
| PCell-F-g1 | FTO | 14 | 3.3 | 100 | 0.73 | 10.35 | 0.65 | 4.91 |
| PCell-F-g2 | FTO | 14 | 3.3 | 200 | 0.74 | 9.24 | 0.64 | 4.38 |
| PCell-I | ITO | 200 | 3.3 | – | 0.64 | 13.03 | 0.32 | 2.67 |
| PCell-I-g2 | ITO | 200 | 3.3 | 200 | 0.73 | 5.69 | 0.54 | 2.24 |

In order to study the total effect of PTL thickness, TCO sheet resistance and gap width on cell performance, a PCell is assembled by inserting a 200 μm Teflon film in original PCell-I. This cell is denoted as PCell-I-g2. Its *J–V* characteristics are listed in Table 3. The PCE of PCell-I-g2 is only 2.24%, which is much smaller than that of PCell-F-t, PCell-I or PCell-F-g2. Therefore, in comparison to the PCE of PCell-F-t, the much smaller PCE of TCell-m can be explained by the synergic effects of its thinner PTL, much larger TCO sheet resistance and wider gap. In other words, the PCE of TCell has potential to be improved if these parameters are improved. This improvement will be carried out in our future works.

### 4.4. Performance comparison of TCell and PCell under increasing light intensity

#### 4.4.1. The temperature

When solar cells are irradiated, the light can be transformed into heat besides electricity [52]. The heat plays important role on the photoelectric characteristics of DSSCs [53,54]. For studying the influence of cell geometry on photo–generated heat, the surface temperatures of photoanode in two typical cells with different geometries are studied. The studied TCell and PCell are TCell-m and PCell-F-t, respectively. The temperature is identified with an infrared thermometer. The measurement is carried out with the same $\theta = 5^{\circ}$ for the two cells. The temperature dependences on light intensity are shown in Fig. 8. It is observed that the temperatures of two cells both increase with increasing light intensity, and the increase rate of TCell-m is smaller than that of PCell-F-t. The smaller increase rate of TCell-m is probably because the tubular geometry is beneficial to heat dissipating compared to the planar counterpart. This can be attributed to the bigger volume of tubular geometry.

#### 4.4.2. The long–term stability of cells

For studying the influence of cell geometry on cell performance in different light intensity, three typical cells are studied for comparison. The three cells are TCell-m, PCell-F-t and PCell-I-g2. The PCell-F-t (or PCell-I-g2) is chosen because of its maximum (or minimum) PCE of PCells in this work. In other words, the PCell-F-t (or PCell-I-g2) can represent the high–efficiency (or low–efficiency) PCell, respectively. In the following study of increasing light intensity, the total irradiated time for one cell tested in each light intensity is less than 1 h, and the maximum irradiated light intensity is 5 Sun. For studying the stability of the three cells in long–term illumination, their *J–V* characteristics are persistently measured under 5 Sun illumination in the range of 1 h. The $V_{OC}$, $J_{SC}$, FF and PCE variation are shown in Fig. 9(a), (b), (c) and (d), respectively. For each parameter, the measured values are normalized by the values obtained at 0 h. The values at 0 h, *i.e.* the values obtained at 5 Sun, can be identified in the cell performance variation with increasing light intensity, which will be shown in the following section. For the three cells, the FF value almost remains constant. The $V_{OC}$, $J_{SC}$ and PCE all decrease with increasing irradiated time. These variation regulations are similar to those reported in literature [53,55]. These can be attributed to the electrolyte evaporation or heat effect [56]. Compared to the $V_{OC}$ and FF variation, the $J_{SC}$ variation is more remarkable. The $J_{SC}$ decrease rate of TCell-m is smaller than those of other two PCells, probably because the heat effect for the TCell is weaker, as discussed in Section 4.4.1. After 1 h, the PCE values of three cells all decrease by about 5%. The stability order is TCell-m > PCell-I-g2 > PCell-F-t. The PCell-I-g2 is more stable than PCell-F-t. This is probably because the lights have more probability to penetrate through the thinner PTL of PCell-I-g2, and then give weaker heat effect.

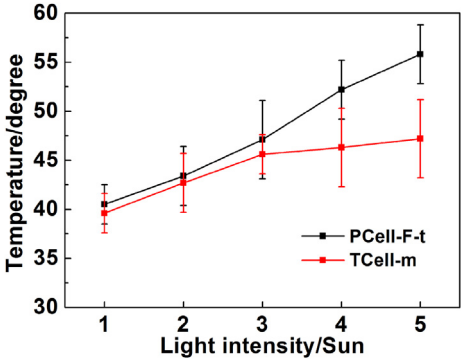


**Fig. 8.** The temperature variation with increasing light intensity for PCell-F-t and TCell-m. The results with standard error are obtained from five measurements and error bars are presented.

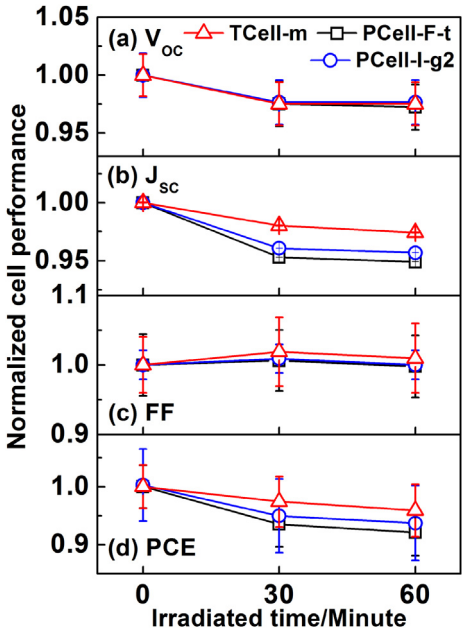


**Fig. 9.** The variation of (a) $V_{OC}$, (b) $J_{SC}$, (c) FF and (d) PCE for TCell-m, PCell-F-t and PCell-I-g2 with the increase of irradiation time under 5 Sun. The results with standard error are obtained from five samples and error bars are presented.

#### 4.4.3. The study of cell performance under increasing light intensity

With increasing light intensity, the variations of *J–V* characteristics for the three typical cells are studied. Their $V_{OC}$, $J_{SC}$, FF and PCE variations are shown in Fig. 10(a), (b), (c) and (d), respectively. For each parameter, the measured values are normalized by the values obtained at 1 Sun illumination, as shown in Section 4.2.3 and Table 3. For the parameter of $V_{OC}$, $J_{SC}$, FF or PCE, it is observed that the variation affected by irradiated time (Fig. 9) is much smaller than that affected by light intensity (Fig. 10). Therefore, the irradiated time effect is ignored in the following study. The study here focuses more the performance comparison between TCell and PCell, so the comparison between two PCells (PCell-F-t and PCell-I-g2) is not carried out in detail.

As shown in Fig. 10(a), with increasing light intensity, the $V_{OC}$ values of PCells (PCell-F-t and PCell-I-g2) decrease, and that of TCell-m increases. It is reported that decreasing $V_{OC}$ can be caused by increasing charge recombination rate affected by increasing temperature, and increasing $V_{OC}$ can be caused by increasing charge generation rate affected by increasing light intensity [57]. As

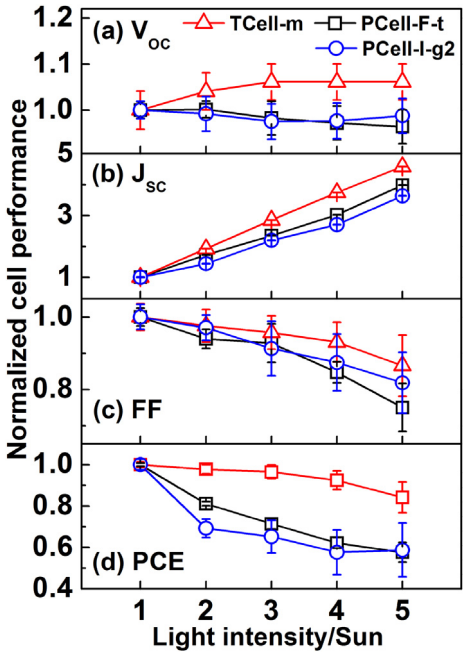


**Fig. 10.** The variation of (a) $V_{OC}$, (b) $J_{SC}$, (c) FF and (d) PCE for TCell-m, PCell-F-t and PCell-I-g2 with the increase of light intensity. The results with standard error are obtained from five samples and error bars are presented.

discussed in Sections 4.4.1 and 4.4.2, the temperature plays more serious negative effect on PCell (PCell-F-t or PCell-I-g2) compared to TCell-m. Therefore, the decreasing $V_{OC}$ of PCell-F-t (or PCell-I-g2) can be attributed to the greater negative effect from increasing temperature, and the increasing $V_{OC}$ of TCell-m can be attributed to the greater positive effect from increasing light intensity.

As shown in Fig. 10(b), the $J_{SC}$ values of three cells all increase with increasing light intensity, and the increase rate of TCell-m is bigger than that of PCell (PCell-F-t or PCell-I-g2). As discussed in Section 4.2.2 and 4.2.3, the increasing $J_{SC}$ can be attributed to increasing $P_A$, increasing charge generation rate or decreasing charge recombination rate. As discussed in entire Section 4.2, the tubular geometry of TCell-m is demonstrated an effective light-trapping to absorb light. Therefore, it can be deduced that the tubular geometry of TCell-m is beneficial to gain increasing $P_A$ value and increasing charge generation rate with increasing light intensity. On the other hand, it can be deduced the tubular geometry of TCell-m is adverse to gain decreasing charge recombination rate with increasing light intensity because of its large cell area. Therefore, here the bigger increase rate of $J_{SC}$ for TCell-m can be attributed to the dominant effect of increasing $P_A$ value or increasing charge generation rate.

As shown in Fig. 10(c), the FF values of three cells all decrease with increasing light intensity, and the decrease rate of TCell-m is smaller than that of PCell (PCell-F-t or PCell-I-g2). Under

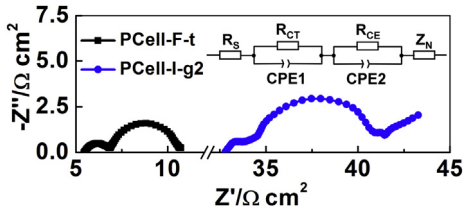


**Fig. 11.** The Nyquist plots of PCell-F-t and PCell-I-g2. The inset is the equivalent circuit for PCell-I-g2.

**Table 4**
The fitted equivalent resistances of PCell-F-t and PCell-I-g2 under 1 Sun.

| Cell | $R_S$ (Ω cm²) | $R_{CT}$ (Ω cm²) | $R_{CE}$ (Ω cm²) | $Z_N$ (Ω cm²) |
|---|---|---|---|---|
| PCell-F-t | 5.43 | 1.38 | 3.80 | – |
| PCell-I-g2 | 32.80 | 1.40 | 7.15 | 7.78 |

illumination, a high electron accumulation must be expected because photo–generated electrons are not extracted at the electrode contact [58–60]. This electron accumulation can increase charge recombination rate, and then limit charge diffusion in photoanode thereby to decrease the FF value [14,55]. Therefore, here the smaller decrease rate of FF for TCell-m is probably because its large volume can effectively relieve this diffusion limitation.

As shown in Fig. 10(d), the resulting PCE of TCell-m remains about 85% of its original value, even if the irradiated light intensity increases from 1 to 5 Sun. In contrast, the PCE of PCells decreases to about 60% of its original value, whether the original PCE of PCell is high (PCell-F-t) or low (PCell-I-g2). This demonstrates that the TCell is relatively stable even in intense light illumination compared to a planar counterpart.

With increasing light intensity, the equivalent resistance variations of the three cells are studied. Under 1 Sun, the Nyquist plots of PCell-F-t and PCell-I-g2 are shown in Fig. 11. The equivalent circuit of PCell-F-t is shown in the inset of Fig. 4 (b), and that of PCell-I-g2 is shown in the inset of Fig. 11, where the $Z_N$ is the diffusion impedance of electrolyte [61]. The corresponding equivalent resistances are listed in Table 4. It is observed that the $R_S$ value of PCell-F-t is bigger than that of TCell-m, which can be attributed to the thicker PTL and assembly method of PCell-F-t. The PCell-F-t is formed by a mask covered planar DSSC, as described in Section 2.3. The photo–generated electrons in PCell-F-t need pass through excessive TCO region under mask before they reach the external circuit. Therefore, the $R_S$ value of PCell-F-t is relatively big.

The $R_S$, $R_{CT}$ and $R_{CE}$ variation are shown in Fig. 12(a), (b) and (c), respectively. The $Z_N$ variation is not discussed because only PCell-I-g2 shows $Z_N$ and lack of reference from other cells. It is observed that the $R_S$, $R_{CT}$ and $R_{CE}$ values for these cells all decrease with increasing light intensity. For these cells, compared to the decrease rate of $R_S$ or $R_{CT}$, that of $R_{CE}$ is more remarkable. The $R_{CE}$ decrease rate of TCell-m is bigger than that of PCell (PCell-F-t or PCell-I-g2).

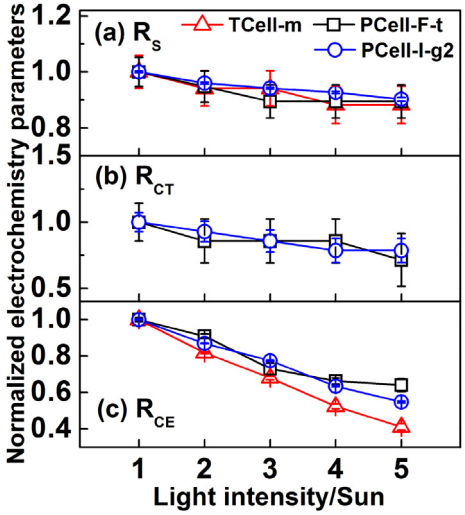


**Fig. 12.** The variation of (a) $R_S$, (b) $R_{CT}$ and (c) $R_{CE}$ for TCell-m, PCell-F-t and PCell-I-g2 with the increase of light intensity. The results with standard error are obtained from five samples and error bars are presented.

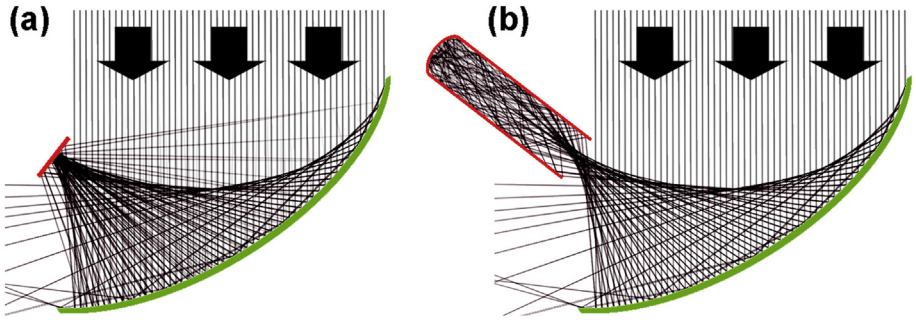


**Fig. 13.** An illustration of optical paths in condenser solar cell system with light collector of (a) PCell and (b) TCell.

On the basis of discussions in Section 4.2.2 and 4.2.3, it can be deduced that the $R_{CE}$ variation is affected by three factors including $P_A$, charge generation rate and charge recombination rate. Here, the bigger $R_{CE}$ decrease rate of TCell-m is probably because the positive effect from increasing $P_A$ (or increasing charge generation rate) exceeds the negative effect from increasing charge recombination rate. For the PCells, the relatively small $R_{CE}$ variation of PCell-F-t can be attributed to the relatively strong negative effect of increasing charge recombination rate because of heat, as discussed in Section 4.4.2, and the relatively small $R_{CE}$ variation of PCell-I-g2 can be attributed to the relatively weak positive effect of increasing $P_A$ because of its thinner PTL, as discussed in Section 4.2.2. A smaller $R_{CE}$ value is proposed beneficial to cell performance, as discussed in Section 4.2.2 and 4.2.3. Therefore, the variation regulations of $R_{CE}$ further confirm those of cell performance as discussed in the first part of this section.

## 5. Application prospect

In this work, the TCell with appropriate structure is demonstrated an effective light-trapping DSSC under parallel illumination generated by a Solar Simulator. However, in real condenser solar cell system, the solar cell collector is generally irradiated by converged light. The light paths in condenser solar cell system with PCell and TCell collector are plotted in Fig. 13(a) and (b), respectively. It is clear that the TCell can more effectively harvest light with its light-trapping geometry, compared to the PCell. Therefore, based on the discussions above, it can be deduced that the TCell has potential as an effective light collector with stable PCE in wide light intensity range in real condenser solar cell system.

## 6. Conclusion

A semi-closed TCell is developed and demonstrated an effective light-trapping when its opening end is irradiated. Its hollow opening end can effectively make the lights enter tube cavity without light loss, and rear closed end can effectively prevent lights from leaking out, especially at small light incidence angle. The maximum PCE of 2.54% is achieved for TCell when its PTL is 3 mm length and 3.3 μm thickness, and light incidence angle is 5°. This PCE has potential to be improved if the device structure is further optimized. Experiment, calculation and light path analysis demonstrate that the tubular geometry is beneficial to light absorption, charge transport and heat dissipation, in comparison to its planar counterpart. The PCE of TCell can remain about 85% of its original value even if the irradiated light intensity increases from 1 to 5 Sun, in contrast, that of planar counterpart decreases to about 60% of its original value. This feature makes the TCell has potential as an effective light collector in condenser solar cell system.

## Acknowledgments

This work was supported by the 973 Program (2011CB933300) of China, the National Natural Science Foundation of China (61376013, J1210061), the Natural Science Foundation of Jiangsu Province (BK20131186), and Wuhan Science & Technology Bureau (2013010501010141).

## References

[1] A. Yella, H.-W. Lee, H.N. Tsao, C. Yi, A.K. Chandiran, M.K. Nazeeruddin, E.W.-G. Diau, C.-Y. Yeh, S.M. Zakeeruddin, M. Grätzel, Science 334 (2011) 629–634.
[2] W. Zeng, G.J. Fang, B.R. Li, Z.Q. Liu, T.Y. Han, J. Wang, F.W. Liu, P.F. Fang, X.Z. Zhao, D.C. Zou, ACS Appl. Mater. Interfaces 5 (2013) 7101–7108.
[3] P.L. Qin, G.J. Fang, W. Zeng, X. Fan, Q. Zheng, F. Cheng, J.W. Wan, X.Z. Zhao, Sol. Energy Mat. Sol. C 95 (2011) 3311–3317.
[4] F. Cheng, G.J. Fang, X. Fan, H.H. Huang, Q. Zheng, P.L. Qin, H.W. Lei, Y.F. Li, Sol. Energy Mat. Sol. C 110 (2013) 63–68.
[5] J. Burschka, N. Pellet, S.-J. Moon, R. Humphry-Baker, P. Gao, M.K. Nazeeruddin, M. Gratzel, Nature 499 (2013) 316–319.
[6] S.M. Lee, S.J. Lee, S.C. Choi, J.M. Kim, S.H. Kim, D.W. Lee, Opt. Express 20 (2012) A908–A915.
[7] G.D. Barber, P.G. Hoertz, S.-H.A. Lee, N.M. Abrams, J. Mikulca, T.E. Mallouk, P. Liska, S.M. Zakeeruddin, M. Grätzel, A. Ho-Baillie, M.A. Green, J. Phys. Chem. Lett. 2 (2011) 581–585.
[8] Y. Fu, Z. Lv, S. Hou, H. Wu, D. Wang, C. Zhang, Z. Chu, X. Cai, X. Fan, Z.L. Wang, D. Zou, Energy Environ. Sci. 4 (2011) 3379–3383.
[9] K.J. Moon, S.W. Lee, Y.H. Lee, J.H. Kim, J.Y. Ahn, S.J. Lee, D.W. Lee, S.H. Kim, Nanoscale Res. Lett. 8 (2013) 283.
[10] J. Bohannon, Science 315 (2007), 792–792.
[11] H. Baig, K.C. Heasman, T.K. Mallick, Renew. Sust. Energy Rev. 16 (2012) 5890–5909.
[12] S. Khelifi, L. Ayat, A. Belghachi, Eur. Phys. J. Appl. Phys. 41 (2008) 115–119.
[13] D.-W. Liu, I.C. Cheng, J.Z. Chen, H.-W. Chen, K.-C. Ho, C.-C. Chiang, Opt. Express 20 (2012) A168–A176.
[14] T. Trupke, P. Würfel, I. Uhlendorf, J. Phys. Chem. B 104 (2000) 11484–11488.
[15] M. Toivola, L. Peltokorpi, J. Halme, P. Lund, Sol. Energy Mat. Sol. C 91 (2007) 1733–1742.
[16] S. Choi, E.-n.-r. Cho, S.-m. Lee, Y.-w. Kim, D.-w. Lee, Opt. Express 19 (2011) A818–A823.
[17] K. Ryu, J.G. Rhee, K.M. Park, J. Kim, Sol. Energy 80 (2006) 1580–1587.
[18] A.J. Frank, N. Kopidakis, J. van de Lagemaat, Coord. Chem. Rev. 248 (2004) 1165–1179.
[19] N. Kopidakis, K.D. Benkstein, J. van de Lagemaat, A.J. Frank, J. Phys. Chem. B 107 (2003) 11307–11315.
[20] A. Bahrami, S. Mohammadnejad, S. Soleimaninezhad, Opt. Quant. Electron 45 (2013) 161–197.
[21] S. Zhong, B. Liu, Y. Xia, J. Liu, J. Liu, Z. Shen, Z. Xu, C. Li, Sol. Energy Mat. Sol. C 108 (2013) 200–204.
[22] W.-R. Wei, M.-L. Tsai, S.-T. Ho, S.-H. Tai, C.-R. Ho, S.-H. Tsai, C.-W. Liu, R.-J. Chung, J.-H. He, Nano Lett. 13 (2013) 3658–3663.
[23] S. Choi, E.N.R. Cho, S.M. Lee, Y.W. Kim, D.W. Lee, Opt. Express 19 (2011) A710–A715.
[24] S. Guldin, S. Huttner, M. Kolle, M.E. Welland, P. Muller-Buschbaum, R.H. Friend, U. Steiner, N. Tetreault, Nano Lett. 10 (2010) 2303–2309.
[25] K.M. Guo, M.Y. Li, X.L. Fang, X.L. Liu, B. Sebo, Y.D. Zhu, Z.Q. Hu, X.Z. Zhao, J. Power Sources 230 (2013) 155–160.
[26] S. Foster, S. John, Energy Environ. Sci. 6 (2013) 2972–2983.
[27] B. Weintraub, Y. Wei, Z.L. Wang, Angew. Chem. Int. Ed. 48 (2009) 8981–8985.
[28] Y.P. Fu, Z.B. Lv, H.W. Wu, S.C. Hou, X. Cai, D. Wang, D.C. Zou, Sol. Energy Mat. Sol. C 102 (2012) 212–219.

[29] C.F. Pan, W.X. Guo, L. Dong, G. Zhu, Z.L. Wang, Adv. Mater. 24 (2012) 3356–3361.
[30] J. Usagawa, S.S. Pandey, S. Hayase, M. Kono, Y. Yamaguchi, Appl. Phys. Express 2 (2009) 062203.
[31] Z. Lv, Y. Fu, S. Hou, D. Wang, H. Wu, C. Zhang, Z. Chu, D. Zou, Phys. Chem. Chem. Phys. 13 (2011) 10076.
[32] H. Tao, G.J. Fang, W.J. Ke, W. Zeng, J. Wang, J. Power Sources 245 (2014) 59–65.
[33] Y.M. Liu, X.H. Sun, Q.D. Tai, H. Hu, B.L. Chen, N. Huang, B. Sebo, X.Z. Zhao, J. Power Sources 196 (2011) 475–481.
[34] B. Peng, G. Jungmann, C. Jager, D. Haarer, H.W. Schmidt, M. Thelakkat, Coord. Chem. Rev. 248 (2004) 1479–1489.
[35] Y. Li, E.D. Peterson, H.H. Huang, M.J. Wang, D. Xue, W.Y. Nie, W. Zhou, D.L. Carroll, Appl. Phys. Lett. 96 (2010) 243505.
[36] Y. Li, W. Zhou, D. Xue, J.W. Liu, E.D. Peterson, W.Y. Nie, D.L. Carroll, Appl. Phys. Lett. 95 (2009) 203503.
[37] Y. Li, H.H. Huang, M.J. Wang, W.Y. Nie, W.X. Huang, G.J. Fang, D.L. Carroll, Sol. Energy Mat. Sol. C 98 (2012) 273–276.
[38] R. Gomez, P. Salvador, Sol. Energy Mat. Sol. C 88 (2005) 377–388.
[39] X. Fan, Z.Z. Chu, F.Z. Wang, C. Zhang, L. Chen, Y.W. Tang, D.C. Zou, Adv. Mater. 20 (2008) 592–595.
[40] K. Fan, T. Peng, B. Chai, J. Chen, K. Dai, Electrochim. Acta 55 (2010) 5239–5244.
[41] K.S. Kim, H. Song, S.H. Nam, S.M. Kim, H. Jeong, W.B. Kim, G.Y. Jung, Adv. Mater. 24 (2012) 792–798.
[42] C.Y. Neo, J. Ouyang, J. Power Sources 241 (2013) 647–653.
[43] M.G. Kang, K.S. Ryu, S.H. Chang, N.G. Park, J.S. Hong, K.J. Kim, B. Kor, Chem. Soc. 25 (2004) 742–744.
[44] W. Zeng, G.J. Fang, X.Q. Wang, Q. Zheng, B.R. Li, H.H. Huang, H. Tao, N.S. Liu, W.J. Xie, X.Z. Zhao, D.C. Zou, J. Power Sources 229 (2013) 102–111.
[45] J. Halme, P. Vahermaa, K. Miettunen, P. Lund, Adv. Energy Mater. 22 (2010) E210–E234.
[46] Q. Wang, S. Ito, M. Gratzel, F. Fabregat-Santiago, I. Mora-Sero, J. Bisquert, T. Bessho, H. Imai, J. Phys. Chem. B 110 (2006) 25210–25221.
[47] W. Zeng, G.J. Fang, T.Y. Han, B.R. Li, N.S. Liu, D.S. Zhao, Z.Q. Liu, D.Y. Wang, X.Z. Zhao, D.C. Zou, J. Power Sources 245 (2014) 456–462.
[48] T.L. Ma, X.M. Fang, M. Akiyama, K. Inoue, H. Noma, E. Abe, J. Electroanal. Chem. 574 (2004) 77–83.
[49] Z. Yanyan, K. Jirapon, K. Hyunsu, N. Sun Young, Y. Haibin, J. Sungho, Nanotechnology 24 (2013) 045401.
[50] E. Ramasamy, W.J. Lee, D.Y. Lee, J. Sung-Song, J. Power Sources 165 (2007) 446–449.
[51] C. Lee, W. Kang, M.J. Ko, K. Kim, N.G. Park, J. Sol. Energy Asme. 132 (2010) 021104.
[52] H.H. Huang, Y.A. Li, M.J. Wang, W.Y. Nie, W. Zhou, E.D. Peterson, J.W. Liu, G.J. Fang, D.L. Carroll, Sol. Energy 85 (2011) 450–454.
[53] M. Berginc, U. Opara Krašovec, M. Jankovec, M. Topi&ccaron, Sol. Energy Mat. Sol. C 91 (2007) 821–828.
[54] J.-H. Yum, R. Humphry-Baker, S.M. Zakeeruddin, M.K. Nazeeruddin, M. Grätzel, Nano Today 5 (2010) 91–98.
[55] P.J. Sebastian, A. Olea, J. Campos, J.A. Toledo, S.A. Gamboa, Sol. Energy Mat. Sol. C 81 (2004) 349–361.
[56] P.M. Sommeling, M. Späth, H.J.P. Smit, N.J. Bakker, J.M. Kroon, J. Photochem. Photobiol. A 164 (2004) 137–144.
[57] H.J. Snaith, L. Schmidt-Mende, M. Grätzel, M. Chiesa, Phys. Rev. B 74 (2006) 045306.
[58] C. Longo, A.F. Nogueira, M.-A. De Paoli, H. Cachet, J. Phys. Chem. B 106 (2002) 5925–5930.
[59] G. Franco, J. Gehring, L.M. Peter, E.A. Ponomarev, I. Uhlendorf, J. Phys. Chem. B 103 (1999) 692–698.
[60] J. van de Lagemaat, N.G. Park, A.J. Frank, J. Phys. Chem. B 104 (2000) 2044–2052.
[61] S.Q. Huang, H.C. Sun, X.M. Huang, Q.X. Zhang, D.M. Li, Y.H. Luo, Q.B. Meng, Nanoscale Res. Lett. 7 (2012) 222.